ACS APPLIED MATERIALS & INTERFACES

Research Article

www.acsami.org

Dual Precursor Atmospheric Plasma Deposition of Transparent Bilayer Protective Coatings on Plastics

Siming Dong, Zhenlin Zhao, and Reinhold H. Dauskardt*

Department of Materials Science and Engineering, Stanford University, Stanford, California 94305-2205, United States

ABSTRACT: We demonstrate a dual organic and inorganic precursor method to deposit transparent organosilicate protective bilayer coatings on poly methyl methacrylate (PMMA) substrates with atmospheric plasma deposition in ambient air. The bottom layer was a hybrid organosilicate adhesive layer deposited with dual organic 1,5-cyclooctadiene (CYC) and widely used inorganic tetraethoxysiline (TEOS) precursors. The selection of the organic CYC precursor allowed incorporation of a carbon chain in the organosilicate adhesive layer, which resulted in improved adhesion. The top layer was a dense silica coating with high Young's modulus and hardness deposited with TEOS. The deposited bilayer structure showed ~100% transparency in the visible light wavelength region, twice the adhesion energy, and five times the Young's modulus of commercial polysiloxane sol–gel coatings.

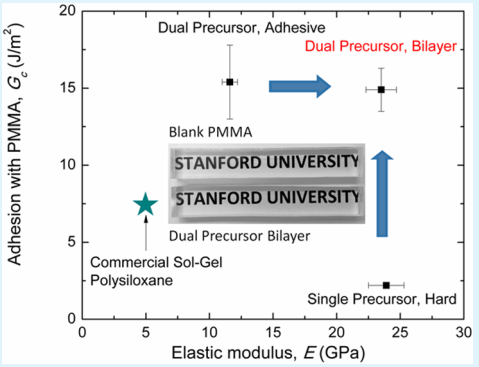

KEYWORDS: *transparent multifunctional coatings, atmospheric plasma, organosilicate coatings, dual precursor method, adhesion*

1. INTRODUCTION

Transparent protective coatings play an increasingly important role in technologies such as flexible electronics, photovoltaics, and plastic glazing and moldings.[1,2] Deposition of effective transparent protective coatings with both high hardness and adhesion properties is an important technical challenge. Transparent silica protective coatings have been deposited using sol–gel techniques, but the interfacial adhesion with plastics is generally not determined[3−6] or is in the low range of ~2−8 J/m^2.[7,8] In addition, the reported elastic Young's modulus is typically ~5 GPa, and a higher value would suggest improved wear and abrasion properties.

Using a novel atmospheric plasma deposition technique, we recently demonstrated the deposition of hard, adhesive, and transparent bilayer organosilicate coatings on PMMA substrates using a 1,2-bis(triethoxysilyl)ethane (BTESE) precursor. The coatings' adhesion with PMMA was twice that of commercial polysiloxane sol–gel coatings and exhibited a 3-fold increase in Young's modulus.[1] Atmospheric plasma deposition is particularly suitable for controlling the adhesive and bulk properties of transparent protective coatings using a multilayer deposition strategy separately with accurate control of coating thickness and properties.[1] Furthermore, it is a versatile process that enables rapid deposition on large and/or complex substrate shapes without a vacuum chamber or wet chemistry process required with conventional vacuum-based techniques (e.g., atomic layer deposition, chemical vapor deposition, and sputtering) and sol–gel techniques.[9]

In this study, we demonstrate a strategy using dual organic and inorganic precursors for atmospheric plasma bilayer deposition. Compared to the BTESE precursor used in our previous study mentioned above and also compared to the silicate precursors including tetramethylcyclotetrasiloxane (TMCTS) and tetramethyldisiloxane (TMDSO), tetraethoxysiline (TEOS) is a low cost and widely used precursor for silicate coating deposition.[1,2,10] It has relatively higher vapor pressure (~1.5 Torr at 23 °C) which enables a lower delivery temperature. The dense silica coatings deposited using TEOS by atmospheric plasma deposition were shown to have the highest Young's modulus compared to those of other precursors.[2] However, the deposited silica coatings using TEOS have a low adhesion (~2 J/m^2) with polymer substrates such as PMMA. To solve this challenge, we first demonstrate the deposition of a bottom adhesive layer comprising an adhesive organic–inorganic hybrid layer deposited using dual CYC and TEOS precursors. While octadiene precursors were reported to be applied in vacuum plasma deposition to improve the interfacial adhesion with other polymers and organic fibers such as poly *p*-phenylene benzobisoxazole (PBO) and keratinocytes,[11,12] the application of these organic molecules in atmospheric plasma has never been reported. The CYC is volatile at room temperature and reactive during plasma deposition since it has two double bonds in the ring molecular structure which undergoes ring opening and incorporation into the coating molecular network. We show that the addition of the CYC precursor significantly increased the carbon content and plasticity of the deposited coating. A dense silica top layer with high hardness and Young's modulus was then deposited using a single TEOS precursor. The bilayer coating exhibited ~100% transmittance in the visible wavelength region, twice the adhesion energy, and ~5-fold the Young's modulus compared to those of commercial polysiloxane sol–gel coatings.[1,2]

Received: May 27, 2015
Accepted: July 20, 2015
Published: July 20, 2015

DOI: 10.1021/acsami.5b04622
ACS Appl. Mater. Interfaces 2015, 7, 17929−17934

2. EXPERIMENTAL METHODS

2.1. Film Deposition. An atmospheric 13.56 MHz RF plasma source equipped with a scanning sample stage and a 25 mm diameter cylindrical plasma showerhead (Atomflow 400D system, Surfx Technologies LLC, US) was employed. A high-temperature precursor delivery system was used to deliver two precursors.[2] The flow rates of the primary and secondary plasma gases were adjusted by the atmospheric plasma system. The plasma was generated with a primary gas of 20 L/min of high purity compressed He (99.995%) and a secondary gas of O_2 (99.999%). Tetraethyl orthosilicate (TEOS, 99%, Sigma-Aldrich) was used as the silicon source precursor, heated to 80 or 100 °C and then delivered to the flowing postdischarge plasma region with a settled temperature of 135 °C. 1,5-Cycloocatadiene (CYC, 99%, Sigma-Aldrich) was used as the second precursor, kept warm at room temperature (23 °C) with a water bath and delivered to the postdischarge plasma region at room temperature. High purity compressed He was also employed as the dilution and bubbler gas in the precursor delivery system.

Coatings were deposited on military-grade stretched PMMA meeting all requirements of MIL-PRF-25690 (LLAMAS Plastic Inc. CA, USA) with 70 × 10 × 6 mm^3 dimensions and standard silicon wafer substrates with 15 × 15 × 0.78 mm^3 dimensions. The substrates were degreased by isopropanol for cleaning before deposition. The films were deposited at a scan velocity of 50 mm/s and step size of 0.3 mm. The detailed deposition conditions are described in Table 1.

Table 1. Deposition Conditions

parameter	unit	adhesive layer	dense layer
primary plasma gas		He (99.995%)	He (99.995%)
secondary plasma gas		O_2 (99.995%)	O_2 (99.995%)
bubbler and dilution gas		He (99.995%)	He (99.995%)
precursor temperature (TEOS)	°C	100	80,100
precursor temperature (CYC)	°C	0	None
primary gas flow	L/min	20	20
secondary gas flow	L/min	0.3	0.3
bubbler gas flow (TEOS)	L/min	0.08	0.08
bubbler gas flow (CYC)	L/min	0.01, 0.02	none
dilution gas flow	L/min	2.0	2.0
plasma power	W	50	80
deposition distance	mm	5	1
shower head move velocity	mm/s	50	50
step	mm	0.3	0.3

We use different plasma conditions for single layer and bilayer organosilicate deposition.

2.2. Film Characterization. A surface profilometer (Veeco Dektak 150, Veeco Instruments Inc., USA) was used to measure the film thickness on the silicon and PMMA substrate with a film edge created by masking a small region. A UV−vis-NIR spectrophotometer (Cary 6000i, Agilent Technologies Inc., USA) was employed to test the visible transmittance of the films. The average transmittance was calculated by averaging the values obtained for the wavelength in the range of 380 to 800 nm. X-ray photoelectron spectroscopy (XPS, PHI 5000 Versaprobe, Physical Electronics Inc., USA) was applied to evaluate the composition of the film and the delaminated surface. An Al−K_α (1486 eV) X-ray source with a spot size of ∼1 mm was equipped (pass energy, 117.4 eV; scan range, 0−1000 and 1 eV/step). Prior to the measurement, surface atmospheric contaminants were removed by ion sputtering for 3 min. An argon ion beam was applied to sputter off the hybrid thin film, with settings of 1 kV, 0.5 μA, and 1 mm × 1 mm sputter spot. The angle between the detector and the sample surface was 45°. The chemical bonds in the coating were characterized using IR spectroscopy and Raman spectroscopy. The IR spectrum was recorded as power dispersions in KBr using a Nexus 670 FT-IR (reflectance mode) for an average of 200 cycles. Mid-IR in the wavelength range from 600 to 4000 cm^{-1} was probed at a resolution of 4 cm^{-1}. Coatings on silicon substrates were characterized in transmission mode at the Brewster angle of the silicon substrate. The Raman scattering was measured with a Horiba Jobin-Yvon HR-800 Confocal Raman system. A visible light excitation source (32mw, 512 nm) was used. The Raman spectrum was recorded in the range from 0 to 2000 cm^{-1} for three cycles for every sample with a time step of 5 s. The density, ρ, of the coating was measured by specular X-ray reflectivity (XRR) using a X-ray diffraction devise (X'Pert Pro, Panalytical, Westborough, MA) with a ceramic X-ray tube (wavelength = 0.154 nm) and a high resolution horizontal goniometer (reproducibility = ± 0.001°). The calculation method was described elsewhere.[2] The Young's modulus and hardness were measured by nanoindentation. All of the nanoindentation tests were performed on the coating surfaces using the iNano nanoindentation system fabricated by Nanomechanics, Inc. with a diamond indenter. The hardness and Young's modulus were determined using nanoindentation experiments on coatings deposited on silicon substrates and plotting the resulting Young's modulus and hardness as a function of the indentation depth to account for the mismatch of the elastic properties of the coating and substrate using a method described elsewhere.[13−15] Before testing, a series of indents at various contact depths were performed on fused quartz with a Young's modulus of 72 GPa as a standard sample for calibration.

2.3. Adhesion Measurement. The adhesion energies, G_c, of the deposited organosiicate coatings on the silicon substrates were measured using a double cantilever beam (DCB) specimen. Details of the DCB techniques can be found elsewhere.[16,17] Test specimens were prepared by bonding an identical blank silicon beam onto the hybrid film deposited on an underlying silicon substrate using a thin epoxy layer (<2 μm). The specimen was mounted into an adhesion testing system (Delaminator, DTS company, US) with metal loading tabs glued on two sides of the specimen. The initial crack was introduced from the edge of the sample by applying a tensile load. The specimen was loaded in tension with a displacement rate of 1.0 μm/s until the crack extension and then unloaded.[18]

The adhesion energy of the coating on PMMA was quantified using the asymmetric double cantilever beam (ADCB) test.[18−20] The specimens were prepared by bonding a blank (uncoated) substrate of 3 mm thickness onto a coated substrate of 6 mm thick. The in-plane dimensions of the specimen were 9 mm × 70 mm. The fracture tests were conducted on a micromechanical adhesion test system (DTS Delaminator Test System, DTS Company, Menlo Park, CA) in displacement control mode. The specimens were loaded at a displacement rate of 5 μm/s in tension to produce controlled crack growth, followed by unloading. The load was measured simultaneously, and the adhesion energy G_c (J/m^2) was calculated. The details can be found elsewhere.[2,19]

3. RESULTS AND DISCUSSION

3.1. Deposition Rate. The dense layer and adhesive layer were individually deposited on silicon and PMMA substrates with different TEOS vaporizing temperatures (80 and 100 °C) and different CYC flow rates (0.01L/min and 0.02L/min). The average deposition rates of the deposited coatings are shown in Table 2. The deposition rates of the adhesive layers using the dual organic and inorganic precursors were ∼2 times the deposition rate of the dense layers deposited using a single TEOS precursor, suggesting that the organic precursor was incorporated into the deposited coating. The deposition rates of the coatings increased with increasing vaporizing temperatures of TEOS and increasing flow rates of CYC. More evidence of the incorporation is presented in the following sections.

3.2. Chemical Composition of Coatings. Using full XPS spectra, the atomic percentages of carbon (C), oxygen (O), and silicon (Si) in the deposited organosilicate dense layer from single TEOS and adhesive layers from dual organic and inorganic precursors with different CYC flow rates are shown in Table 3. The C content increased markedly from 3.6% to 10.8% after

DOI: 10.1021/acsami.5b04622
ACS Appl. Mater. Interfaces 2015, 7, 17929−17934

Table 2. Deposition Rates and Properties of Organosilicate Films Deposited from TEOS and Two Precursors

coating condition	deposition rate (Si, nm/min)	deposition rate (PMMA, nm/min)
dense layer (80 °C)	26 ± 1.1	32 ± 1.3
dense layer (100 °C)	40 ± 0.9	47 ± 2.1
adhesive layer (0.01 L/min CYC)	67 ± 2.2	72 ± 4.7
adhesive layer (0.02 L/min CYC)	82 ± 3.1	97 ± 3.4

Table 3. Compositions of Organosilicate Films Deposited from TEOS and Dual Precursors without Optimized Conditions

elements	dense layer (80 °C)	adhesive layer (0.01 L/min CYC)	adhesive layer (0.02 L/min CYC)
Si	28.6%	24.7%	25.0%
O	67.8%	64.5%	60.6%
C	3.6%	10.8%	14.4%

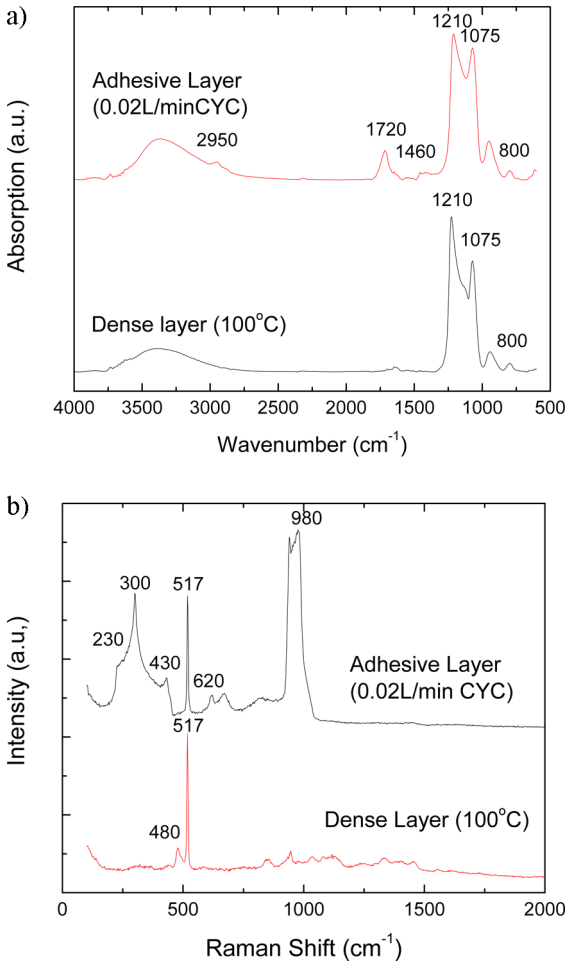

Figure 1. (a) FTIR spectrum for single layer coatings deposited from a TEOS precursor and two precursors. (b) Raman spectrum for coatings deposited from a TEOS precursor and two precursors with excitation wavelengths of 512 nm.

using a dual precursor with 0.01 L/min CYC flow rate suggesting that a more carbon-included organic component has been incorporated into the coating molecular network. The carbon content of deposited coatings also increase to ∼15% with 0.02L/min

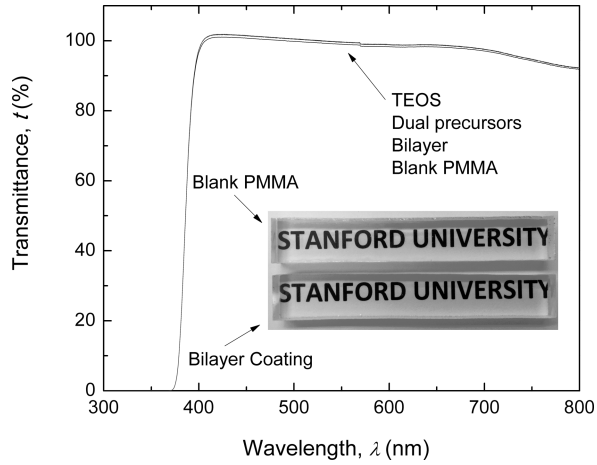

Figure 2. Transmittance spectrum with wavelength from 300 to 800 nm and an optical image for a blank PMMA substrate, PMMA with coatings deposited by single TEOS, dual precursors, and bilayer coatings.

organic CYC flow rate, which means that dual precursor strategy is successful in increasing and controlling the carbon content in the deposited adhesive layer coatings.

The chemical forms of carbon and silicon species present in the adhesive and dense layers were investigated by FTIR (Figure 1a). The coating conditions are shown in the figure. Strong bands associated with the asymmetric stretching, bending, and rocking modes of the Si−O−Si bond were observed at ∼1075 and 800 cm^{-1} in both spectra.[21−23] The relative intensity difference of the bands at ∼1075 cm^{-1} of two coatings resulted from different molecular network structures of Si−O−Si. The FTIR spectra confirmed the XPS results that the dense layer deposited using a single TEOS precursor was almost pure silica with significantly low carbon content (∼4%), while the spectra of the adhesive layer deposited using dual precursors showed a lower peak of 1075 cm^{-1} due to higher carbon content and a less dense Si−O−Si network in the coatings.[2] This is also demonstrated by the coating density result in Table 2. The peak at ∼930 cm^{-1} was attributed to Si−OH stretching mode,[24] which is consistent with coatings deposited using plasma enhanced chemical vapor deposition (PECVD) at reduced temperature.[24−26] The dual precursor adhesive layer showed obvious peaks at ∼1470 cm^{-1} and ∼2950 cm^{-1} which are nearly absent in the dense layer deposited using a single TEOS precursor. The peak at ∼1470 refers to Si−O−C species, and the peak at ∼2950 results from sp^3 C−H stretching vibrations.[2,27] Appearance of these peaks suggests that the organic component in the coating deposited by dual organic and inorganic precursors may form a connected − Si−O−C− structure and improve the network connectivity of the coatings. The peak at ∼1725 cm^{-1} was attributed to polar C═O stretching mode which indicates that some organic component is in an oxidative state in the adhesive layer deposited by the dual organic and inorganic precursors method.[2,28] The broad band peaks at ∼3400 cm^{-1} in both spectra are due to an O−H stretching vibration that resulted from terminated hydroxyl groups in the molecular network.[2,25]

The Raman spectrum of the deposited adhesive and dense layer are presented in Figure 1b. The deposition conditions are the same as those of the layers investigated by FTIR. The peak at 517 cm^{-1} appears in both spectra refers to multiphonon scattering from the silicon substrate.[29] The wide band with a

DOI: 10.1021/acsami.5b04622
ACS Appl. Mater. Interfaces 2015, 7, 17929−17934

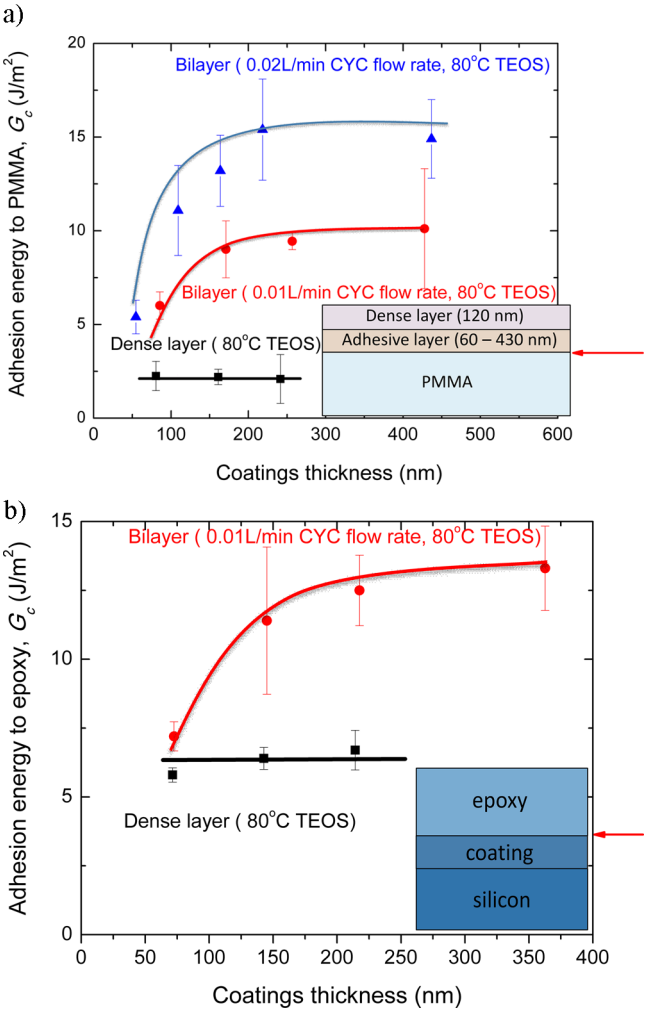

Figure 3. Adhesion energy G_c of deposited coatings (a) on PMMA as a function of coating thickness and (b) on a silicon to epoxy layer as a function of coating thickness.

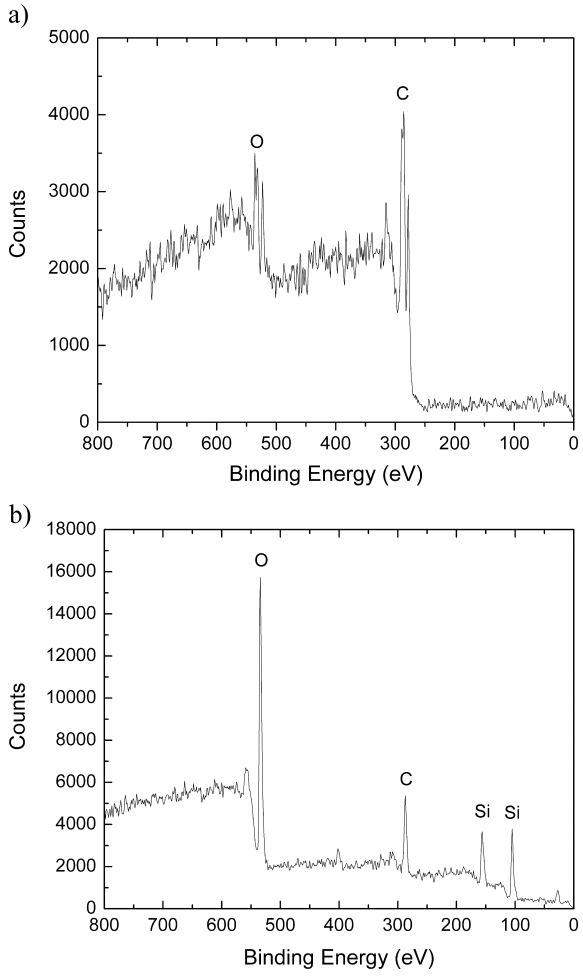

Figure 4. Elemental XPS analysis of the fracture surface of the coatings deposited on PMMA, (a) coated substrate side and (b) opposite side, showing delamination at the PMMA/adhesive organosilicate interface.

maximum at about 230 cm^{-1} can be correlated with scissoring in the [$SiO_{4/2}$] tetrahedron.[30] The 624 cm^{-1} peak with weak intensity corresponds to the position of a maximum of a D2 line observed for dense bulk silica reported in the literature (D, G, and T bands in the silica Raman spectrum are dependent on excitation wavelength; the D band usually shows depressive behavior in visible excitation light).[31,32] All of these peaks can be found in the thin film state SiO_2 but are missing in the bulk SiO_2.[33] This indicates that the adhesive layer deposited using the dual precursors behaves more like a less dense film, while the dense layer deposited using the single TEOS precursor behaves more like a denser bulk material. The wide peak at ~980 cm^{-1} is assigned to the Si−O−CH_2 bond symmetric −Si−O−C− vibration,[34] which again conforms that the organic component in the coating deposited by dual precursors may form a connected −Si−O−C− organosilicate network, also evident from the FTIR results.

3.3. Transmittance Properties. The PMMA substrates employed showed a ≥ 90% transmission in the visible light region (380−800 nm), and no detectable difference in the transmittance spectrum was observed after deposition of the single and bilayer coatings as shown in Figure 2. All of the deposited coatings in this work therefore showed ~100% transmittance in the visible wavelength region.

3.4. Adhesion Properties. The variation of adhesion energy G_c to PMMA substrates of the dense silica layer deposited using a single TEOS precursor and bilayer coatings deposited using dual precursors with different organic CYC flows rates as a function of the coating thickness is presented in Figure 3a. The bilayer coatings deposited using dual organic and inorganic precursors show a significant increase in adhesion energy when compared to that of coatings deposited using single TEOS precursor. These adhesion data were for the organosilicate and PMMA interface, as evidenced by the XPS elemental composition of the fractured surface after adhesion testing (Figure 4). On the substrate side of the fracture surface, no silicon peak was detected. On the opposite side, there was obvious silicon content (~20 atom %). The increase of adhesion resulted from increased carbon content incorporation (form Si−O−C chain) and could form both Si−C and C−C bonds with the polymer substrate. However, the dense layer can only form a limited Si−C bond.[2]

The incorporation of a reactive organic precursor also prevents overoxidation of the polymer substrate during the deposition process especially for PMMA, whose overexposure to plasma has previously been shown to promote the formation of a low-molecular-weight layer and decrease adhesion.[1] The increase of adhesion also resulted from increased molecular bridging that dissipates energy by molecular relaxation in a

DOI: 10.1021/acsami.5b04622
ACS Appl. Mater. Interfaces 2015, 7, 17929−17934

Table 4. Carbon Content, Density, and Mechanical Properties of Hard Silica Coating and Adhesive Organosilicate Coating in the Bilayer Structure

coating condition	carbon content (%)	density (g/cm^3)	Young's modulus (GPa)	hardness (GPa)	adhesion (J/m^2)
dense (top, 80 °C)	3.6%	1.91 ± 0.02	23.7 ± 1.4	2.2 ± 0.1	2.2 ± 0.2
adhesive (bottom,0.02 L/min CYC)	14.4%	1.72 ± 0.01	11.6 ± 0.6	1.5 ± 0.1	15.4 ± 2.4
bilayer			surface:23.5 ± 1.2	surface:2.2 ± 0.1	14.9 ± 1.4

plastic deformation zone near the crack tip during coating delamination.[35−37] The plastic zone size in thick coatings is mainly determined by intrinsic coating properties including the yield stress and ductility of the coating. However, in a thin coating the plastic zone size is constrained by the coating thickness itself, which limits the amount of plastic energy dissipated in the plastic zone. As a result, the adhesion value, G_c, of the coatings deposited from dual precursors increases with increasing coating thickness, and G_c increases with increasing organic CYC flow rates since higher carbon content (Table 3) and a larger plasticity effect can be achieved in the coating. The highest G_c was ∼15 J/m^2, which was twice the adhesion of typical commercial sol−gel siloxane coatings. The adhesion energy, G_c, of coatings deposited using a single TEOS precursor does not vary significantly with coating thickness because of low carbon content and plasticity in the coatings as shown in the XPS result (Table 3).

The adhesion energy G_c for dense silica coatings and bilayer coatings deposited with a 0.01 L/min CYC flow rate on silicone substrate is presented in Figure 3b. The crack propagated at the organosilicate coating/epoxy interface, which is similar to the XPS result of organosilicate coating/PMMA interface (Figure 4). On the substrate side of the fracture surface, very high silicon content (∼20%) was detected. On the opposite side, nearly no silicon peak was detected. The maximum adhesion energy with epoxy layer of coatings deposited from dual organic and inorganic precursors (∼13.3 J/m^2) is 2 times that for coatings deposited from TEOS (∼6.7 J/m^2), which conformed to the adhesion trend for the coatings deposited on PMMA. The increasing trend of adhesion for deposited coatings using dual precursors with an epoxy layer is also in accordance with the adhesion result for the PMMA substrate because of the plasticity effect.

3.5. Coating Density and Mechanical Properties. The coating density and mechanical properties for bilayer coatings deposited using TEOS and dual organic and inorganic precursors are presented in Table 4. The dense layer deposited using single a TEOS precursor with shorter distance, lower precursor flow, and higher power exhibited the higher density of 1.91 g/cm^3, a Young's modulus of 23.7 GPa, and a hardness of 2.2 GPa, but its adhesion energy with PMMA is as low as 2.2 J/m^2, as shown in Figure 3a. The high density, Young's modulus, and hardness of this dense hard layer resulted from a highly connected bulky Si−O−Si molecular network as evidenced by FTIR spectra in Figure 1 and with a low carbon remnant (∼3.6%) as shown in Table 4. Coatings deposited using a dual precursor with higher distance, higher precursor flow, and lower power have a higher adhesion (∼15.4 J/m^2) with lower density, Young's modulus, and hardness. The significantly improved adhesion was related to the higher carbon content (∼14.4%) and the incorporation of carbon chain into the coating's molecular network as discussed previously. The Young's modulus and hardness of the bilayer coatings show inconsistent values through the film as presented in Table 4. The Young's modulus and hardness on the top part of the bilayer coatings have a larger value than the values of the bottom layer, which is the evidence to confirm the existence of the bilayer structure. The overall bilayer coating properties are summarized in Figure 5. The bilayer coatings show twice the adhesion energy and five times the Young's modulus of commercial polysiloxane sol−gel coatings.

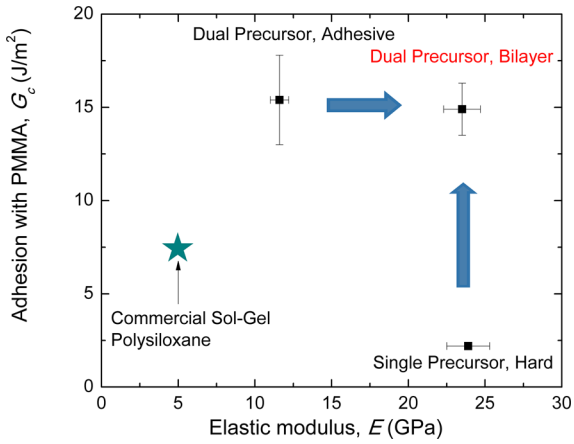

Figure 5. Relationship between Young's modulus and adhesion energy with PMMA for the top, bottom, and bilayer deposited by atmospheric plasma deposition, and the commercial sol−gel polysiloxane coatings.

4. CONCLUSIONS

We successfully demonstrated the strategy of using dual organic and inorganic precursors to deposit organosilicate transparent multifunctional bilayer coatings on PMMA substrates with atmospheric plasma deposition in ambient air. The bottom adhesive layer deposited using dual precursors significantly increased the adhesion energy with the PMMA substrate, and the top hard silica layer showed high Young's modulus and hardness. The bilayer coating combined high adhesion energy, Young's modulus, and hardness at the same time and functioned as an integrated layer. The deposited bilayer structure showed twice the adhesion energy and five times the Young's modulus of commercial polysiloxane sol−gel coatings.

AUTHOR INFORMATION

Corresponding Author

*E-mail: dauskardt@stanford.edu.

Notes

The authors declare no competing financial interest.

ACKNOWLEDGMENTS

We thank the US Department of Energy for their financial support under Contract No. DE-FG02-07ER46391.

REFERENCES

(1) Cui, L.; Lionti, K.; Ranade, A.; Larson-Smith, K.; Dubois, G.; Dauskardt, R. H. Highly Transparent Multifunctional Bilayer Coatings

DOI: 10.1021/acsami.5b04622
ACS Appl. Mater. Interfaces 2015, 7, 17929−17934

on Polymers Using Low-Temperature Atmospheric Plasma Deposition. *ACS Nano* **2014**, *8*, 7186−7191.
(2) Cui, L.; Ranade, A.; Matos, M.; Pingree, L.; Frot, T.; Dubois, G.; Dauskardt, R. H. Atmospheric Plasma Deposited Dense Silica Coatings on Plastics. *ACS Appl. Mater. Interfaces* **2012**, *4*, 6587−6598.
(3) Tanglumlert, W.; Prasassarakich, P.; Supaphol, P.; Wongkasemjit, S. Hard-coating Materials for Poly(methyl methacrylate) from Glacidoxypropyltrimethoxysilane-modified Silatrane via a Sol-gel Process. *Surf. Coat. Technol.* **2006**, *200*, 2784−2790.
(4) Sepeur, S.; Kunze, N.; Werner, B.; Schmidt, H. UV Curable Hard Coatings on Plastics. *Thin Solid Films* **1999**, *351*, 216−219.
(5) Chan, C. M.; Cao, G. Z.; Fong, H.; Sarikaya, M.; Robinson, T.; Nelson, L. Organic/inorganic Hybrid Sol-gel Derived Hard Coatings on Plstics. *MRS Online Proc. Libr.* **1999**, *576*, 319−324.
(6) Kao, Y.; Hong, F. Improved Adhesion of PMSQ Hard Coatings on Po Substrates. *J. Coat. Technol. Res.* **2011**, *8*, 779−783.
(7) Lionti, K.; Cui, L.; Volksen, W.; Duaskardt, R. H.; Dubois, G.; Toury, B. Independent Control of Adhesive and Bulk Properties of Hybrid Silica Coatings on Polycarbonate. *ACS Appl. Mater. Interfaces* **2013**, *5*, 11276−11280.
(8) Shenton, M.; Lovell-Hoare, M.; Stevens, G. Adhesion Enhancement of Polymer Surfaces by Atmospheric Plasma Treatment. *J. Phys. D: Appl. Phys.* **2001**, *34*, 2754−2760.
(9) Hiller, D.; Zierold, R.; Bachmann, J.; Alexe, M.; Yang, Y.; Gerlach, J. W.; Stesmans, A.; Jivanescu, M.; Müller, U.; Vogt, J.; et al. Low Temperature Silicon Dioxide by Thermal Atomic Layer Deposition: Investigation of Material Properties. *J. Appl. Phys.* **2010**, *107*, 064314−064314−10.
(10) Dong, S.; Watanabe, M.; Dauskardt, R. H. Conductive Transparent TiNx/TiO2 Hybrid Films Deposited on Plastics in Air Using Atmospheric Plasma Processing. *Adv. Funct. Mater.* **2014**, *24*, 3075−3081.
(11) Sugihara, H.; Jones, F. R. Promoting the Adhesion of High-performance Polymer Fibers Using Functional Plasma Polymer Coatings. *Polym. Compos.* **2009**, *30*, 318−327.
(12) Haddow, D. B.; France, R. M.; Short, R. D.; Dawson, R. A.; Legget, G. J.; Cooper, E. Comparison of Proliferation and Growth of Human Keratinocytes on Plasma Copolymers of Acrylic Acid/1,7-octadiene and Self-assembled Monolayers. *J. Biomed. Mater. Res.* **1999**, *47*, 379−387.
(13) Oliver, W. C.; Pharr, G. M. Measurement of Hardness and Elastic Modulus by Instrumented Indentation: Advances in Understanding and Refinements to Methodology. *J. Mater. Res.* **2004**, *19* (1), 3−20.
(14) Oliver, W. C.; Pharr, G. M. An Improved Technique for Determining Hardness and Elastic Modulus Using Load and Displacement Sensing Indentation Experiments. *J. Mater. Res.* **1992**, *7*, 1564−1583.
(15) Han, S.; Guyer, E.; Nix, W. Extracting Thin Film Hardness of Extremely Compliant Films on Stiff Substrates. *Thin Solid Films* **2011**, *519*, 3221−3224.
(16) Dauskardt, R. H.; Lane, M.; Ma, Q.; Krishna, N. Adhesion and Debonding of Multi-layer Thin Film Structures. *Eng. Fract. Mech.* **1998**, *61*, 141−162.
(17) Matsuda, Y.; King, S. W.; Bielefeld, J.; Xu, J.; Dauskardt, R. H. Fracture Properties of Hydrogenated Amorphous Silicon Carbide Thin Films. *Acta Mater.* **2012**, *60* (2), 682−691.
(18) Kanninen, M. F. Augmented Double Cantilever Beam Model for Studying Crack-Propagation and Arrest. *Int. J. Fract.* **1973**, *9*, 83−92.
(19) Kamer, A.; Larson-Smith, K.; Pingree, L.; Dauskardt, R. H. Adhesion and Degradation of Hard Coatings on Poly (methyl methacrylate) Substrates. *Thin Solid Films* **2011**, *519*, 1907−1913.
(20) Suo, Z. G.; Hutchinson, J. W. Sandwich Test Specimens for Measuring Interface Crack Toughness. *Mater. Sci. Eng., A* **1989**, *107*, 135−143.
(21) Theil, J.; Tsu, D.; Watkins, M.; Kim, S.; Lucovsky, G. Local Bonding Environments of Si−OH Groups in SiO_2 Deposited by Remote Plasma Enhanced Chemical Vapor Deposition and Incorporated by Postdeposition Exposure to Water Vapor. *J. Vac. Sci. Technol., A* **1990**, *8*, 1374−1381.
(22) Nowling, G.; Yajima, M.; Babayan, S.; Moravej, M.; Yang, X.; Hoffman, W.; Hicks, R. Chamberless Plasma Deposition of Glass Coatings on Plastic. *Plasma Sources Sci. Technol.* **2005**, *14*, 477−484.
(23) Katsamberis, D.; Browall, K.; Iacovangelo, C.; Neumann, M.; Morgner, H. Highly Durable Coatings for Automotive Polycarbonate Glazing. *Prog. Org. Coat.* **1998**, *34*, 130−134.
(24) Rau, C.; Kulisch, W. Mechanisms of Plasma Polymerization of Various Silico-organic Monomers. *Thin Solid Films* **1994**, *249*, 28−37.
(25) Schafer, J.; Foest, R.; Quade, A.; Ohl, A.; Weltmann, K. Local Deposition of SiOx Plasma Polymer Films by a Miniaturized Atmospheric Pressure Plasma Jet (APPJ). *J. Phys. D: Appl. Phys.* **2008**, *41*, 194010−194010−9.
(26) Huang, C.; Liu, C.-H.; Wu, S. Surface Characterization of the SiO*x* Films Prepared by a Remote Atmospheric Pressure Plasma Jet. *Surf. Interface Anal.* **2009**, *41*, 44−48.
(27) Matos, M.; Ilharco, L.; Almeida, R. The Evolution of TEOS to Silica Gel and Glass by Vibrational Spectroscopy. *J. Non-Cryst. Solids* **1992**, *147*, 232−237.
(28) Pandey, K. A study of Chemical Structure of Soft and Hardwood and Wood Polymers by FTIR Spectroscopy. *J. Appl. Polym. Sci.* **1999**, *71*, 1969−1975.
(29) Temple, P.; Hathaway, C. Multiphonon Raman Spectrum of Silicon. *Phys. Rev. B* **1973**, *7*, 3685−3696.
(30) Borowicz, P.; Taube, A.; Rzodkiewicz, W.; Latek, M.; GieraBtowska, S. Raman Spectra of High-κ Dielectric Layers Investigated with Micro-Raman Spectroscopy Comparison with Silicon Dioxide. *Sci. World J.* **2013**, *2013*, 208081−208087.
(31) Yoshikawa, M.; Nagai, N.; Matsuki, M.; Fukuda, K.; Katagiri, G.; Ishida, H.; Ishitani, A.; Nagai, I. Raman Study of Interface Phonons in GaAs/AlAs Quantum Wells: Resonance with the E2-h2 Exciton. *Phys. Rev. B: Condens. Matter Mater. Phys.* **1992**, *46*, 7169−7174.
(32) Kingma, K.; Hempley, R. Raman Spectroscopic Study of Microcrystalline Silica. *Am. Mineral.* **1994**, *79*, 269−273.
(33) Borowicz, P.; Latek, M.; Rzodkiewicz, W.; Łaszcz, A.; Czerwinski, A.; Ratajczak. Deep-Ultraviolet Raman Investigation of Silicon Oxide: Thin Film on Silicon Substrate Versus Bulk Material. *Adv. Nat. Sci.: Nanosci. Nanotechnol.* **2012**, *3*, 045003−045003−7.
(34) Licht, K.; Reich, P. *Literature Data for Infrared, Raman and N.M.R. Spectra of Silicon, Germanium, Tin and Lead Organic Compounds*; Deutscher Verlag der Wissenschaften: Berlin, Germany, 1971.
(35) Matsuda, Y.; Ryu, I.; King, S.; Bielefeld, J.; Dauskardt, R. H. Toughening Thin-Film Structures with Ceramic-Like Amorphous Silicon Carbide Films. *Small* **2014**, *10*, 253−257.
(36) Litteken, C.; Dauskardt, R. H. Adhesion of Polymer Thin-Films and Patterned Lines. *Int. J. Fract.* **2003**, *120*, 475−485.
(37) Rowland, H. D.; King, W. P.; Pethica, J. B.; Cross, G. L. W. Molecular Confinement Accelerates Deformation of Entangled Polymers during Squeeze Flow. *Science* **2008**, *322*, 720−724.

DOI: 10.1021/acsami.5b04622
ACS Appl. Mater. Interfaces 2015, 7, 17929−17934